Drug Design, Development and Therapy

Dovepress
Taylor & Francis Group

Open Access Full Text Article

ORIGINAL RESEARCH

Shatai Heji Mitigates Sjögren Disease-Induced Xerostomia by Regulating AQP5, NF-κB, and p38 MAPK Signaling Pathwaysaff

Fangbin Liu*, Jiyuan Chen*, Chunai Gong*, Minyan Chen, Gang Yang, Chun Chen, Ru Yao, Shengnan Li, Rong Wang, Yongfang Yuan

Department of Pharmacy, Shanghai Ninth People's Hospital, Shanghai Jiao Tong University School of Medicine, Shanghai, People's Republic of China

*These authors contributed equally to this work

Correspondence: Rong Wang; Yongfang Yuan, Department of Pharmacy, Shanghai Ninth People's Hospital, Shanghai JiaoTong University School of Medicine, 280 Mohe Road, Shanghai, 201999, People's Republic of China, Tel/Fax +86-021-56786907, Email wangrong198521@126.com; nmxyyf@126.com

Drug Design, Development and Therapy downloaded from https://www.dovepress.com/
For personal use only.

Introduction: Xerostomia, commonly caused by Sjögren disease (SjD) or head and neck radiotherapy, significantly impairs patients' quality of life, yet effective treatments remain limited. Traditional Chinese Medicine (TCM) offers promising alternatives due to its favourable efficacy and low toxicity. Shatai Heji (STHJ), a compound TCM formulation designed to nourish yin and invigorate qi, shows therapeutic potential for xerostomia. This study aimed to establish quality control standards for STHJ and evaluate its pharmacodynamics, safety, and mechanisms of action in models of xerostomia.

Methods: A qualitative identification method was developed for the twelve herbal components of STHJ, with quantification of active constituents, focusing on quality markers for Astragalus and Rehmannia. Xerostomia was induced in Sprague–Dawley (SD) rats using a muscarinic receptor antagonist, and in BALB/c mice with SjD. Histological examination of major organs and salivary glands was performed, and aquaporin-5 (AQP5) expression in submandibular glands was assessed via Western blotting and immunohistochemistry. Therapeutic effects were evaluated through salivary secretion, glandular weight, and biochemical markers. In SjD mice, submandibular gland immunofluorescence and ELISA were used to assess inflammatory cytokines (TNF-α, TNF-β, IFN-γ, IL-6) and autoantibodies (anti-SSA/Ro, anti-SSB/La). Western blotting was used to analyse NF-κB and MAPK p38 pathway activation. Acute toxicity was assessed in SD rats.

Results: STHJ significantly improved xerostomia symptoms, increased salivary output, upregulated AQP5, and preserved glandular morphology. It reduced fibrosis, suppressed inflammatory cytokine expression, and inhibited immune cell infiltration. Mechanistically, STHJ attenuated activation of NF-κB and MAPK p38 pathways. No acute toxicity was observed.

Conclusion: This is the first study to establish quality control standards for STHJ and to demonstrate its anti-inflammatory and immunomodulatory effects in xerostomia models. The findings suggest that STHJ may serve as a safe and effective therapeutic option for xerostomia associated with SjD and other conditions.

Keywords: shatai heji, STHJ, xerostomia, sjögren disease, SjD, submandibular glands, anti-inflammatory, AQP5

Introduction

Xerostomia, defined as the subjective sensation of dry mouth due to decreased salivary secretion, is a common clinical symptom rather than a distinct disease entity. It frequently occurs in patients with Sjögren disease (SjD), diabetes, after head and neck radiotherapy, or as a side effect of medications and anxiety.[1–3] Reduced expression of aquaporin 5 (AQP5) in salivary glands, particularly the submandibular gland, is closely associated with impaired water transport and the development of xerostomia symptoms. SjD is a chronic autoimmune disease marked by lymphocytic infiltration and progressive damage to exocrine glands. Over 80% of patients experience xerostomia and dry eye symptoms, and

Received: 4 March 2025
Accepted: 1 August 2025
Published: 9 September 2025

© 2025 Liu et al. This work is published and licensed by Dove Medical Press Limited. The full terms of this license are available at https://www.dovepress.com/terms.php and incorporate the Creative Commons Attribution – Non Commercial (unported, v4.0) License (http://creativecommons.org/licenses/by-nc/4.0/). By accessing the work you hereby accept the Terms. Non-commercial uses of the work are permitted without any further permission from Dove Medical Press Limited, provided the work is properly attributed. For permission for commercial use of this work, please see paragraphs 4.2 and 5 of our Terms (https://www.dovepress.com/terms.php).

Graphical Abstract

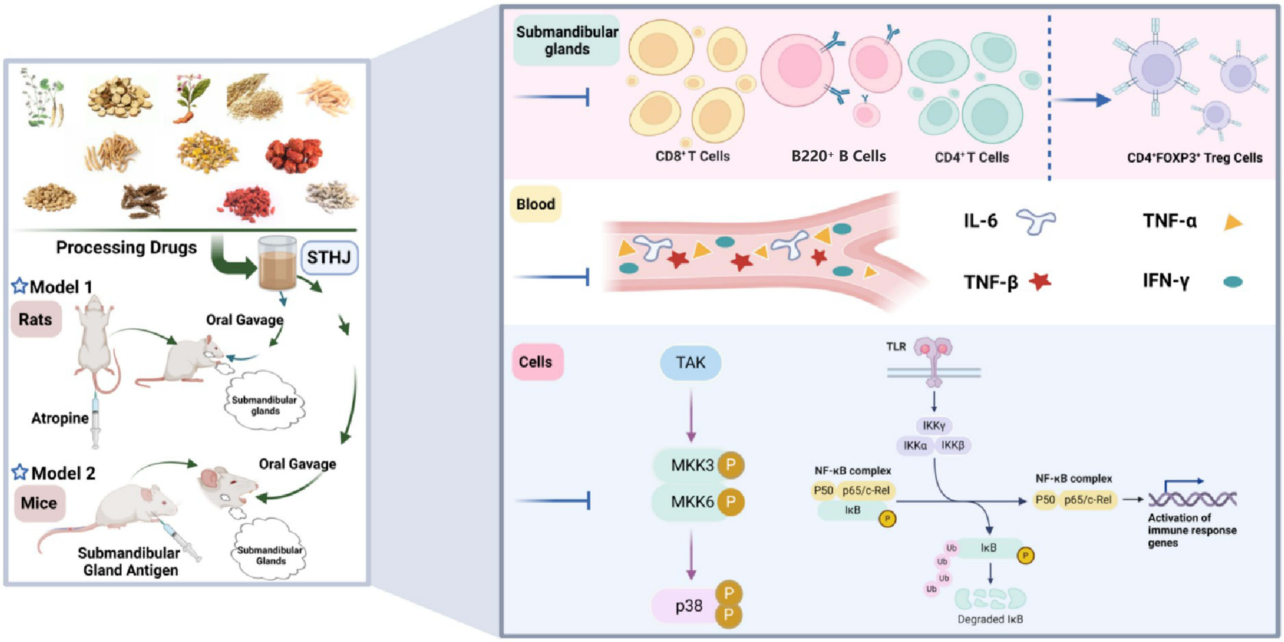

approximately one-third exhibit systemic involvement, including the skin, joints, kidneys, and nervous and respiratory systems.[4] Importantly, SjD is also associated with an elevated risk of non-Hodgkin lymphoma.[5,6]

Despite the burden of xerostomia, there remains a lack of effective long-term treatments. The cholinergic agonist pilocarpine is currently used to stimulate salivation but suffers from poor receptor selectivity and systemic side effects, providing only transient symptomatic relief.[7] This underscores the need for safer, more effective therapeutic alternatives targeting the pathophysiology of xerostomia, particularly in autoimmune settings such as SjD.

Shatai Heji (STHJ) is a traditional Chinese medicine formulation composed of twelve herbal ingredients: *Radix Adenophorae, Radix Pseudostellariae, Radix Rehmanniae, Radix Astragali, Herba Dendrobii, Radix Ophiopogonis, Fructus Lycii, Bombyx Batryticatus, Prunella Vulgaris, Triticum Aestivum, Fructus Jujubae* and *Radix Glycyrrhizae*. These components possess documented anti-inflammatory and immunomodulatory properties. For example, hydrophilic polysaccharides from *Radix Pseudostellariae* enhance immune activity,[8] while acteoside from *Radix Rehmanniae* modulates IL-10 production via the TLR4/PI3K pathway.[9,10] *Radix Astragali* polysaccharides have been shown to improve cardiac function in SjD rats through the Keap1-Nrf2/ARE axis.[11] Clinical studies have also confirmed the immunomodulatory effects of STHJ.[12] Our previous research demonstrated that STHJ administration significantly increased thymus and spleen indices, B cell and natural killer (NK) cell activity, while reducing $CD8^+$ T, $CD8^+CD122^+$ T, NKT, and γδT cell activity in cyclophosphamide-treated mice. In summary, STHJ effectively alleviated cyclophosphamide-induced immunosuppression by balancing lymphocyte subsets and cytokine expression.[13] These findings suggest that STHJ has a potent immunomodulatory effect, mitigating excessive activation of the immune system in autoimmune disease models and protecting tissues and organs from damage. Thus, STHJ shows potential in treating xerostomia caused by SjD, although its therapeutic effects and underlying immunomodulatory mechanisms remain to be fully elucidated.

Therefore, this study was designed to comprehensively evaluate the therapeutic potential of STHJ for treating xerostomia. We first aimed to refine its quality control standards by establishing a TLC-based qualitative identification method for its twelve herbal components, alongside the quantification of key active ingredients in *Radix Astragali* and

Radix Rehmanniae. We then assessed its pharmacodynamics, safety, and underlying mechanisms in two animal models: an M receptor antagonist-induced xerostomia model in SD rats and an SjD model in BALB/c mice. We further explored the effects of STHJ on inflammatory response modulation, fibrosis, immune infiltration, and the NF-κB and MAPK p38 pathways, to provide experimental evidence supporting its application in SjD-related xerostomia.

Materials and Methods

Reagents and Instruments

STHJ was prepared by the Department of Pharmaceutical Products, Shanghai Ninth People's Hospital, Shanghai Jiao Tong University School of Medicine, Batch No. 20230712. Calycosin glucoside ($C_{22}H_{22}O_{10}$, CAS No: 20633–67-4, B644412, purity ≥ 98%) was purchased from Boer Co., Ltd. (Shanghai, China). Ethyl acetate ($C_4H_8O_2$, CAS No: 141–78-6, R003519, purity ≥ 99%), glycyrrhizic acid ammonium salt ($C_{42}H_{65}NO_{16}$, CAS No: 53956–04-0, R094641, purity ≥ 98%), p-anisaldehyde ($C_8H_8O_2$, CAS No: 123–11-5, R003195, purity ≥ 98%), and rosmarinic acid ($C_{18}H_{16}O_8$, CAS No: 20283–92-5, R006901, purity ≥ 98%) were purchased from Shanghai Linen Technology Development Co., Ltd. Dendrobine ($C_{16}H_{25}NO_2$, CAS No: 2115–91-5, D302778, purity ≥ 98%) was purchased from Aladdin Holdings Group Co., Ltd. (Beijing, China). Oleanolic acid ($C_{30}H_{48}O_3$, CAS No: 508–02-1, M53740, purity ≥ 98%) and betulinic acid ($C_{30}H_{48}O_3$, CAS No: 2115–91-5, F20491, purity ≥ 98%) were purchased from Shanghai Mineral Chemical Technology Co., Ltd. Primary antibodies against β-actin (Cat# 4970S), IKBα (Cat# 4812S), p-IKBα (Cat# 9246S), p-p65 (Cat# 3033S), p65 (Cat# 8242S), p-p38 MAPK (Cat# 4511S), p38 MAPK (Cat# 8690S), Ikkβ (Cat# 8943S), and p-Ikkα/β (Cat# 2697S) were purchased from Cell Signaling Technology (Shanghai, China). Primary antibodies against AQP5 (GB113318-50) were purchased from Wuhan Servicebio Technology Co., Ltd. (Shanghai, China). Goat anti-rabbit IgG (H+L) Fluor 594-conjugated antibody (Cat# S0006, RRID: AB_2843436; Affinity Biosciences) and goat anti-rabbit IgG (H+L) horseradish peroxidase (HRP) (Cat# S0001, RRID: AB_2839429; Affinity Biosciences) for Western blotting, and goat anti-rabbit IgG (H+L) Fluor488-conjugated antibody (Cat# S0018, RRID: AB_2846215; Affinity Biosciences) for immunofluorescence staining, were also provided by Fushen Biotech Co., Ltd. (Shanghai, China). The dye 4′,6-diamidino-2-phenylindole (DAPI, G1012), DAB colour reagent (DAB, G1212), Mouse TNF-alpha Uncoated ELISA Kit (88–7324), Mouse IFN-gamma ELISA Kit (GEM0006), Mouse TNF-β ELISA Kit (RD-RX20853-96), and Mouse IL-6 Uncoated ELISA Kit (88–7064) were purchased from Wuhan Servicebio Technology Co., Ltd. (Shanghai, China). Anti-SSA/Ro ELISA Kit (ED-AN22989) and anti-La/SSB Ab ELISA Kit (A102279-96) were purchased separately from Lunchangshuo Biotechnology Co., Ltd (Xiamen, China) and Fusheng Industrial Co., Ltd (Shanghai, China). A BCA Protein Assay Kit was purchased from Baitai Biotechnology Co., Ltd. (Shanghai, China). Male BALB/c mice were purchased from Biyuan Biotechnology Co., Ltd. (Shanghai, China) and Sprague-Dawley (SD) rats were purchased from Ziyuan Laboratory Animal Technology Co., Ltd. (Hangzhou, China).

Preparation and Identification of STHJ

STHJ is composed of twelve traditional Chinese medicines, including *Radix Adenophorae, Radix Pseudostellariae, Radix Rehmanniae, Radix Astragali, Herba Dendrobii, Radix Ophiopogonis, Fructus Lycii, Bombyx Batryticatus, Prunella Vulgaris, Triticum Aestivum, Fructus Jujubae and Radix Glycyrrhizae*. These medicines were separately decocted twice with water at an 8-fold and 6-fold volume. The first decoction lasted 1.5 h, and the second lasted 1 h. The resulting decoctions were filtered, combined, and left to stand for over 12 h. The supernatant was then concentrated to approximately 1000 mL. Sodium benzoate (3 g) and sucrose (200 g) were added while the solution was hot, thoroughly mixed, and diluted to 1000 mL. The final product is a clear brown liquid with a sweet and slightly bitter taste. Identification of the preparation was performed following the guidelines in the 2020 edition of the Chinese Pharmacopoeia (Part IV). Detailed procedures are provided in Sections 1-3 of the Supplementary Material.

Quality Control of STHJ

Determination of Relative Density: According to the standard, the relative density should not be less than 1.08 (Chinese Pharmacopoeia, 2020, Part IV, General Rule 0601). A sufficient amount of STHJ was taken and tested at 20°C using a densitometer or pycnometer. The results were recorded to ensure compliance with the standard.

pH Measurement: The pH should range between 4.0 and 6.0 (Chinese Pharmacopoeia, 2020, Part IV, General Rule 0631). The pH of an appropriate amount of STHJ was measured using a calibrated pH meter. The results were recorded to ensure the pH fell within the specified range.

Volume Check: According to the standard, the difference between the filled volume and the labelled volume must not exceed 1 unit, and the filled volume must not be less than 95% of the labelled volume. Five samples were taken, and the contents of each were poured into a standardised measuring cylinder. The filled volume of each sample was recorded and compared with the labelled volume to ensure compliance.

Content Determination: The content was determined using high-performance liquid chromatography (Chinese Pharmacopoeia, 2020, Part IV, General Rule 0512). Detailed procedures are provided in Sections 4 of the Supplementary Material.

Model Establishment

Male SD rats (7 weeks old, 200–220 g) and BALB/c mice (7 weeks old, 18–22 g) were housed under standard temperature and humidity conditions (21 ± 2°C, relative humidity 50 ± 10%) with a 12-h light/dark cycle. After one week of acclimatisation, the experiments were conducted. All experimental procedures were approved by the Animal Ethics Committee of Shanghai Ninth People's Hospital, affiliated with Shanghai Jiao Tong University School of Medicine (Approval No. SH9H-2023-A798-1; 26 June 2023), and conducted in compliance with the national standards of the People's Republic of China (GB/T 43051–2023: Laboratory animal—General requirements for biosafety in animal experiment; GB/T 42011–2022: Laboratory animals—General code of animal welfare).

Two models were established to assess the therapeutic effects of STHJ on xerostomia:

Model 1: SD Rat Model of M Receptor Antagonist-Induced Xerostomia. Rats were randomly divided into six groups (n = 6): normal control, model control, positive control (pilocarpine), and high-, medium-, and low-dose STHJ groups. To induce the xerostomia model, the M receptor antagonist atropine was administered via tail vein injection at 1 mg/kg. The STHJ groups received doses of 1.5 mL, 1 mL, and 0.5 mL by gavage, respectively. The normal and model control groups received 1 mL of saline by gavage, while the positive control group received pilocarpine at 1 mg/kg by tail vein injection. Following model induction, all treatments were administered immediately. Thirty min after drug administration, a 30 mg dry cotton ball was placed sublingually to absorb saliva, and replaced every 30 min for a total duration of 150 min. The weight difference before and after absorption was used to calculate the amount of saliva secreted. Submandibular glands were collected for protein extraction, and AQP5 expression was measured by Western blot.

Model 2: BALB/c Mouse SjD Model. BALB/c mice were randomly divided into six groups (n = 10): normal control, model control, positive control, and high-, medium-, and low-dose STHJ groups. All mice, except those in the normal control group, underwent modelling. It is reported that autoantigens can mediate the formation of SjD in BALB/c mice.[14] Therefore, we collected submandibular gland autoantigens for the establishment of SjD model. Antigen preparation involved washing the submandibular glands of BALB/c mice with saline containing sodium azide, mincing the tissue, and homogenising it in saline using a high-speed homogeniser. The homogenate was sonicated for 1 h, and the supernatant was collected. The protein antigen concentration was measured using a spectrophotometer. The supernatant was diluted with 0.1 M PBS to 100 μg/mL and mixed with an equal volume of complete Freund's adjuvant (CFA) to prepare the antigen. The antigen was injected subcutaneously into the submandibular glands, footpads, and back of the mice (except for the normal control group), with a total volume of 0.5 mL. Booster injections of the same volume were administered on days 14 and 28.

STHJ administration was initiated on Day 1 and continued daily. The STHJ groups received daily gavage doses of 0.5 mL, 0.2 mL, and 0.1 mL, respectively, while the positive control group received pilocarpine at 1 mg/kg by tail vein injection. The normal and model control groups received 0.1 mL of saline by gavage. Saliva secretion was measured

once weekly. On each measurement day, a 30 mg dry cotton ball was placed under the tongue 30 min after drug administration and replaced every 30 min for 150 min. The weight change was used to calculate the volume of secreted saliva. The schematic diagram of animal model induction is presented in Supplementary Figure S3.

The reporting of all animal experiments adhered to the ARRIVE guidelines 2.0. Animal health and behaviour were monitored daily by trained personnel, and humane endpoints were established. Particular attention was paid to the stress associated with repeated oral gavage during long-term administration, and animals were handled gently and consistently to minimise discomfort. Our sample sizes were based on previous studies investigating similar interventions in xerostomia and SjD animal models, ensuring statistical feasibility and comparability. Animals were randomly assigned to experimental groups using a random number generator. All sample processing, Western blotting, ELISA, and histological analyses were conducted in a blinded manner to minimise experimental bias. Histological slides were coded before evaluation by two independent observers blinded to group identity.

Blood Biochemistry and Haematology

SD rats in Model 1 were anaesthetised using pentobarbital, ensuring they reached a deep anaesthesia stage with no pain response. Blood was collected and transferred into appropriate serum or EDTA anticoagulant tubes. A portion of the blood was promptly used for routine haematology testing. The remaining blood samples were left at room temperature for 30 min to clot naturally, followed by centrifugation to collect the serum. The serum was stored at −20°C or −80°C for subsequent biochemical analysis.

HE and Masson Staining

HE Staining: Sections were immersed in haematoxylin stain for 3–5 min, washed with water, differentiated with a differentiation solution, and washed again. After bluing, the sections were dehydrated in 85% and 95% ethanol, stained with eosin, cleared in xylene, and coverslipped for microscopic observation.

Masson Staining: Paraffin sections were deparaffinised and hydrated, followed by treatment with Masson's trichrome staining solutions. After differentiation, the sections were stained to distinguish collagen fibres (blue) from muscle fibres and fibrin (red). The sections were then dehydrated, cleared in xylene, and coverslipped for microscopic examination.

Immunohistochemistry

Fresh submandibular gland tissues were fixed in 10% neutral formalin, embedded in paraffin, and sectioned into 5-μm-thick slices. For immunohistochemistry (IHC), paraffin sections were first deparaffinised and rehydrated. Antigen retrieval was conducted using citrate buffer (pH 6.0), followed by blocking with 3% bovine serum albumin (BSA). The sections were incubated overnight at 4°C with a rabbit anti-AQP5 primary antibody. On the following day, the sections were treated with a biotin-conjugated secondary antibody, followed by incubation with streptavidin–HRP complex and developed using 3,3′-diaminobenzidine (DAB) substrate. Sections were counterstained with haematoxylin for 3 min, dehydrated, cleared, and coverslipped. Stained sections were observed and imaged using a bright-field microscope (E100; Nikon, Japan).

Immunofluorescence

Paraffin-embedded sections of submandibular gland were deparaffinised using environmentally friendly solvents and rehydrated in a graded ethanol series. Antigen retrieval was performed using citrate buffer (pH 6.0), followed by blocking with 5% BSA. Sections were incubated overnight at 4°C with primary antibodies against CD4, CD8, B220, and FOXP3. After washing, the sections were incubated for 1 h at room temperature with species-appropriate fluorescently labelled secondary antibodies. Nuclei were counterstained with DAPI, and the sections were mounted using anti-fade mounting medium (Vector Laboratories). Autofluorescence quenching was performed where needed. Immunofluorescence images were acquired using a NIKON Eclipse Ti laser scanning confocal microscope (Eclipse C2 software, Nikon, Tokyo, Japan).

Immunofluorescence images were acquired using a confocal microscope under consistent exposure settings and exported as TIFF files. Image analysis was performed in ImageJ using a standardized workflow. Background subtraction

(rolling ball method) and Gaussian filtering were applied to reduce noise. Thresholding (Otsu method) was used to segment signals, and binary masks were created for each marker (eg, CD4, FOXP3, B220). Positive cells were quantified using the "Analyze Particles" tool with consistent size and shape parameters. Fluorescence intensity was assessed by calculating corrected total cell fluorescence (CTCF). All images were processed using the same macro script to ensure consistency across samples.

Focus Scoring

Focus scoring was used to evaluate inflammation and fibrosis in the submandibular glands of BALB/c mice. Tissue sections were stained with Hematoxylin and Eosin (H&E) and assessed under a light microscope. A semi-quantitative score (0–3) was assigned based on the degree of inflammation and immune cell infiltration: 0: No focus or inflammation observed. 1: Mild focal inflammation or slight cell infiltration. 2: Moderate inflammation with moderate infiltration of lymphocytes and immune cells. 3: Severe inflammation with extensive infiltration and clear tissue disruption, possibly with early fibrosis. The Focus Score was assigned by two independent evaluators, and scores were averaged for each group.

ELISA

Whole blood samples from each group were collected and centrifuged at 1000 g for 15 min at 2–8°C within 30 min of collection. The supernatant (serum) was either analysed immediately or aliquoted and stored below −20°C to avoid repeated freeze-thaw cycles. ELISA was performed according to the manufacturer's instructions, ensuring that no water droplets or bubbles were present in the wells. The absorbance was measured at 450 nm with a reference wavelength of 630 nm.

Western Blot

Protein was extracted from submandibular gland tissues using RIPA buffer with protease inhibitors. Protein concentration was determined using the BCA assay. Proteins were separated by SDS-PAGE and transferred to PVDF membranes. Membranes were blocked with 5% non-fat milk and incubated with primary antibodies against p-IKKβ, IKKβ, p-p65, p65, p-p38, p38, and β-actin overnight at 4°C. After washing, the membranes were incubated with HRP-conjugated secondary antibodies. Signals were detected using ECL reagent and captured on an imaging system. The intensity of protein bands was quantified using ImageJ software.

Acute Toxicity Test

SD rats were used as test animals in this study. The rats were randomly divided into four groups: a normal control group, and low-, medium-, and high-dose groups of STHJ, with 6 male rats in each group. The acute toxicity of the compound was evaluated 24 h after administration. STHJ was administered orally via gavage to the SD rats. During the administration period, the rats were monitored for external appearance, behaviour, respiratory status, response to stimuli, and mortality. After 24 h, blood samples were collected from the abdominal aorta for comparison of haematological and biochemical parameters among the groups. Additionally, the heart, liver, spleen, lungs, kidneys, brain, testes, submandibular glands, and thymus were excised from the rats, sectioned, and subjected to HE staining for histopathological examination.

Statistical Analysis

All data are expressed as mean ± standard deviation. Statistical analysis was performed using one-way analysis of variance (ANOVA) followed by Tukey's post hoc test for multiple comparisons. Prior to ANOVA, data were tested for normality using the Shapiro-Wilk test and for homogeneity of variances using Levene's test. Exact *p-value*s are reported in the figure legends or main text where relevant. A *p*-value of less than 0.05 was considered statistically significant. The specific *p*-values are provided in Section 8 of the Supplementary Material. All statistical analyses were conducted using GraphPad Prism 9 (GraphPad Software, San Diego, CA, USA).

Results

Quality Standard Testing of STHJ

STHJ comprises twelve traditional Chinese medicinal ingredients, including *Radix Adenophorae, Radix Pseudostellariae, Radix Rehmanniae, Radix Astragali, Herba Dendrobii, Radix Ophiopogonis, Fructus Lycii, Bombyx Batryticatus, Prunella Vulgaris, Triticum Aestivum, Fructus Jujubae, and Radix Glycyrrhizae*. After processing, it forms a clear brownish liquid with a sweet and slightly bitter taste. To ensure quality control, Thin-layer chromatography (TLC) identification tests were conducted to confirm the presence of specific active compounds corresponding to each medicinal component.

As shown in Figure 1A, the TLC results demonstrated consistent chromatographic or fluorescent spots between the test samples and their reference standards, confirming the presence of active constituents such as catalpol (*Radix Rehmanniae*), astragaloside (*Radix Astragali*), dendrobine (*Herba Dendrobii*), rosmarinic acid (Prunella Vulgaris), glycyrrhizic acid monoammonium salt (*Radix Glycyrrhizae*), among others. These findings verified the compositional consistency and quality of STHJ.

In addition, we investigated the impact of different sucrose concentrations (10%, 15%, 20%) on the relative density and pH. As shown in Figure 1B, the relative density values remained approximately 1.2 (not <1.08), and pH values were maintained at 4.7–4.8, with no significant differences ($p > 0.05$), indicating that sucrose concentration had a minimal impact on quality characteristics. In summary, TLC analysis confirmed the presence of characteristic components in STHJ, matching those in the corresponding reference materials. These findings demonstrate that the composition of STHJ

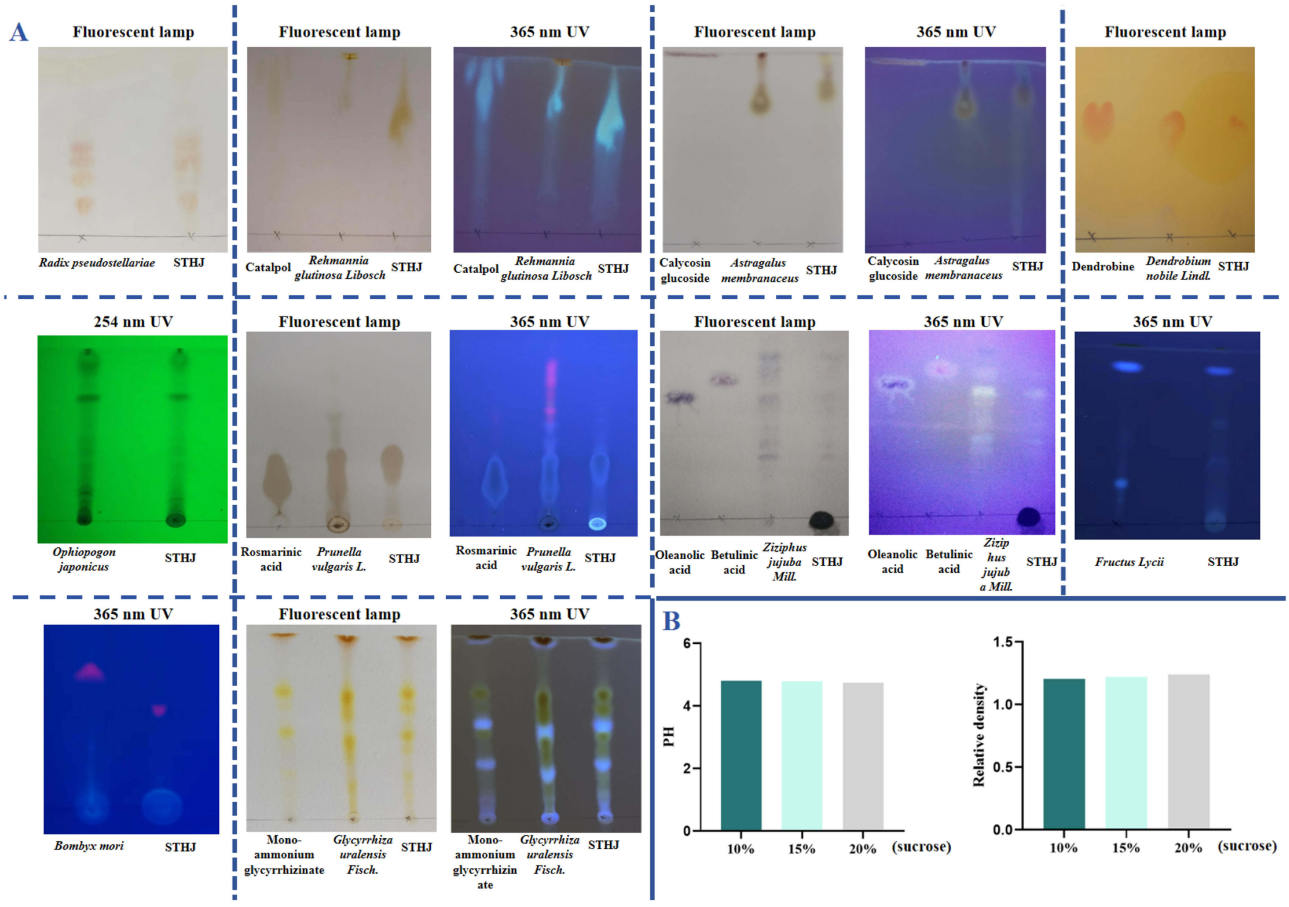

Figure 1 Quality Standard Testing of STHJ. STHJ is composed of twelve traditional Chinese medicinal ingredients, including *Radix Adenophorae, Radix Pseudostellariae, Radix Rehmanniae, Radix Astragali, Herba Dendrobii, Radix Ophiopogonis, Fructus Lycii, Bombyx Batryticatus, Prunella Vulgaris, Triticum Aestivum, Fructus Jujubae and Radix Glycyrrhizae*. (**A**) TLC identification tests were performed to identify the specific components of the medicines. (**B**) Study on the effect of different sucrose concentrations on the pH and relative density of STHJ.

https://doi.org/10.2147/DDDT.S526278

remains consistent and that key active ingredients are reliably detected. Furthermore, the relative density and pH values across different sucrose concentrations (10%, 15%, 20%) met the pharmacopeial standards, indicating that variations in sucrose content had negligible influence on basic quality attributes.

System Suitability Testing

Through TLC analysis of *Radix Astragali* and *Radix Rehmanniae*, identical chromatographic spots were observed at the same positions in both the test sample and reference solutions, indicating good specificity of the test sample. Due to the complexity of STHJ's components, it is difficult to conduct quantitative analysis on all components to evaluate the stability of our prescription process. The combination of Astragalus membranaceus (Huangqi) and Rehmannia glutinosa (Dihuang) has a synergistic effect of tonifying qi and blood, as well as nourishing Yin and benefiting qi. In traditional Chinese medicine compound prescriptions, the two are usually used in combination for the treatment of xerostomia.[15] In addition, the main active ingredients of these two herbs both have standard determination methods in the Chinese Pharmacopoeia (Chinese Pharmacopoeia, 2020, Part I, Page 129 and 315). We then conducted system suitability testing for *Radix Astragali* and *Radix Rehmanniae*. As shown in Tables 1 and 2, within a specific concentration range, the detection signals of astragaloside (0.25–100 μg/mL) from *Radix Astragali* and catalpol (0.3–120 μg/mL) from *Radix Rehmanniae* exhibited a good linear relationship with their concentrations. The linear regression equation for astragaloside was Y = 53,606.0014 X - 13,869.5274, and for catalpol, Y = 4,446.80 X - 1,038.95, with correlation coefficients ≥ 0.9999, indicating good linearity.

As shown in Tables 3 and 4, the repeatability test results indicated good consistency in the detection of astragaloside and catalpol, with low coefficients of variation. The RSD for astragaloside was 0.33%, and for catalpol, it was 0.41%, demonstrating good repeatability. As shown in Tables 5 and 6, stability tests revealed no significant changes in the

Table 1 Linear Study on the Detection Method of Calycosin-7-O-Beta-D-Glucoside

Concentration (μg/mL)	0 25	0.5	1 1	5	10	20	100
Peak area	17255	27,916	54,353	252,176	512,900	1,012,238	5,356,696

Table 2 Linear Precision Study on the Detection Method of Catalpol

Concentration (μg/mL)	0.3	0.6	1.2	6	12	24	120
Peak area	979	2317	4830	24,942	52,773	103,641	532,965

Table 3 Repeatability Study on the Detection Method of Calycosin-7-O-Beta-D-Glucoside

	1	2	3	4	5	6	RSD
Peak area	523914	526,899	522,757	524,217	526,477	526,458	0.0033

Table 4 Repeatability Study on the Detection Method of Catalpol

	1	2	3	4	5	6	Mean value	RSD
Peak area	52935	52,738	53,046	53,106	53,338	53,262	53,070.83	0.0041

Table 5 Stability Study on the Detection Method of Calycosin-7-O-Beta-D-Glucoside

Concentration (μg/mL)	0 h	2 h	4 h	8 h	RSD
0.5	29,078	29,730	29,185	29,328	0.0097
5	266,120	264,438	263,816	265,500	0.0039
20	1,005,826	1,002,742	1,001,917	1,001,375	0.0020

Table 6 Stability Study on the Detection Method of Catalpol

Concentration (μg/mL)	0 h	2 h	4 h	8 h	RSD
0.6	2473	2422	2454	2486	0.0113
6	27,033	26,997	27,042	26,510	0.0096
24	110,606	110,026	110,410	111,542	0.0058

detection results of astragaloside and catalpol within 0 h, 2 h, 4 h, and 8 h, indicating good stability of the test sample within the specified time. As shown in Tables 7 and 8, the spiked recovery test results showed that the average recovery rate for astragaloside was 99.60% and for catalpol was 101.15%, both within the range of 95%–105%, indicating high accuracy of the method. As shown in Tables 9–12, multiple detections of astragaloside and catalpol within the same day exhibited low RSD, demonstrating good within-day precision. The day-to-day precision was also good, with low RSD for astragaloside and catalpol across different days. As shown in Supplementary Material Figures S1 and S2, HPLC analysis confirmed the specificity of Rehmannia and Astragalus membranaceus, with catalpol and calycosin glucoside consistently detected in both raw materials and all STHJ batches, but absent in blank excipients. In summary, the analytical methods for detecting astragaloside and catalpol exhibited good specificity and system suitability. They also showed strong linearity, precision (repeatability and intermediate precision), stability, and satisfactory recovery rates, supporting their suitability for the routine quality control of STHJ.

Table 7 Average Recovery Study on the Detection Method of Calycosin-7-O-Beta-D-Glucoside

	Measured value	Actual Concentration (μg/mL)	Theoretical Concentration (μg/mL)	Recovery Rate (%)	Average Recovery rate (%)	RSD%
80%	1,049,276	19.83	20	99.16	99.60	1.80
	1,042,349	19.70	20	98.52		
	1,035,779	19.58	20	97.90		
100%	1,313,060	24.75	25	99.01		
	1,322,428	24.93	25	99.71		
	1,312,668	24.75	25	98.98		
133%	1,744,746	32.81	32	102.52		
	1,746,971	32.85	32	102.65		
	1,665,631	31.33	32	97.91		

Table 8 Average Recovery Study on the Detection Method of Catalpol

	Measured value	Actual Concentration (μg/mL)	Theoretical Concentration (μg/mL)	Recovery Rate (%)	Average Recovery Rate (%)	RSD%
	74,090	16.90	17	99.38	101.15	1.31
85%	74,427	16.97	17	99.83		
	74,148	16.91	17	99.46		
	90,131	20.50	20	102.51		
100%	90,018	20.48	20	102.38		
	89,172	20.29	20	101.43		
	108,092	24.54	24	102.26		
100%	106,516	24.19	24	100.78		
	108,174	24.56	24	102.33		

https://doi.org/10.2147/DDDT.S526278

Table 9 Within-Day Precision Study on the Detection Method of Calycosin-7-O-Beta-D-Glucoside

Concentration (μg/mL)	0 h	2 h	4 h	8 h	12 h	24 h	RSD
0.5	29,205	29,962	29,414	29,247	29,305	29,111	0.0104
5	264,339	268,463	262,654	265,048	265,728	266,744	0.0075
20	1,030,386	1,031,697	1,032,087	1,028,893	1,033,886	1,022,448	0.0039

Table 10 Within-Day Precision Study on the Detection Method of Catalpol

Concentration (μg/mL)	0 h	2 h	4 h	8 h	12 h	24 h	RSD
0.6	2471	2463	2494	2499	2449	2485	0.0078
6	26,603	26,609	26,921	26,427	26,336	26,334	0.0084
24	107,702	107,726	107,693	108,601	107,820	104,815	0.0122

Table 11 Day to Day Precision Study on the Detection Method of Calycosin-7-O-Beta-D-Glucoside

Concentration (μg/mL)	1 d	2 d	3 d	4 d	RSD
0.5	28,574	28,486	28,460	28,147	0.0066
5	269,445	266,960	267,343	270,953	0.0070
20	1,044,249	1,047,173	1,059,234	1,055,211	0.0066

Table 12 Day to Day Precision Study on the Detection Method of Catalpol

Concentration (μg/mL)	1 d	2 d	3 d	4 d	RSD%
0.6	2354	2349	2371	2323	0.85
6	25,949	26,402	26,186	26,195	0.71
24	104,562	104,992	104,023	103,661	0.56

STHJ Improved Xerostomia in SD Rats Induced by M Receptor Antagonist

To evaluate the therapeutic potential of STHJ in xerostomia, an SD rat model was established using an M receptor antagonist. Rats were allocated into six groups: normal, model, positive control (pilocarpine), and STHJ low-, medium-, and high-dose groups. Saliva secretion, histological changes, AQP5 expression, and serum biochemical indicators were systematically assessed.

Saliva output was measured every 30 min for 150 min. The model group exhibited submandibular gland atrophy and inflammation (Figure 2A), while rats treated with medium and high doses of STHJ showed marked histological improvement and structural preservation. Similar improvements were observed in the positive control group.

Western blot and immunohistochemistry revealed that AQP5 expression was significantly reduced in the model group and increased in a dose-dependent manner following STHJ treatment ($p < 0.05$, Figure 2B–D). Biochemical indices (ALT, AST, UREA, CREA) showed no significant differences among groups (Figure 2C), indicating no apparent liver or kidney damage.

Saliva secretion volume was significantly higher in STHJ-treated groups at 60 min, particularly in the medium- and high-dose groups (Figure 2E). Total saliva volume in the high-dose group was comparable to that of pilocarpine, suggesting that STHJ improves salivary gland function, potentially through upregulation of AQP5.

In summary, these results suggest that STHJ has a beneficial effect in relieving xerostomia symptoms in the SD rat model induced by an M receptor antagonist. The therapeutic mechanism may be associated with upregulated AQP5

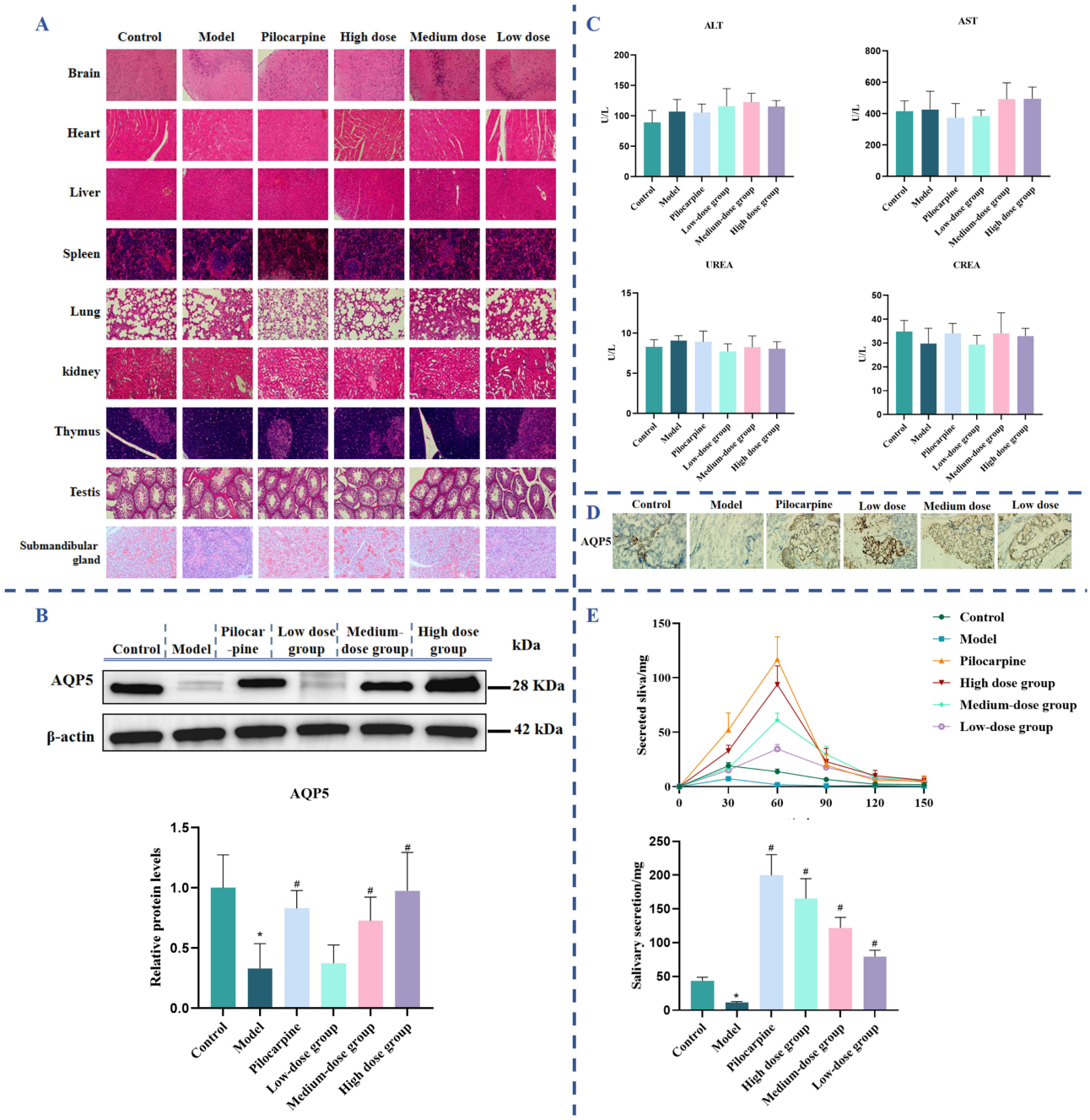

Figure 2 STHJ Improved Xerostomia in SD Rats Induced by M Receptor Antagonist. (**A**) The heart, liver, spleen, lungs, kidneys, brain, testes, submandibular glands, and thymus were harvested from each group of SD rats, sectioned, and subjected to HE staining for histopathological examination. (**B**) The expression levels of AQP5 protein in the submandibular glands of each group were assessed using Western blot analysis. Data are presented as the mean ± S.D., n = 5. $^{*}p < 0.05$ *versus* control group; $^{\#}p < 0.05$ *versus* model group. (**C**) The biochemical parameters, including ALT, AST, UREA, and CREA levels, were measured in each group. Data are presented as the mean ± S.D., n = 6. (**D**) The expression of AQP5 in the submandibular glands of each group of SD rats was evaluated using immunohistochemical staining. (**E**) The total saliva volume over 150 min and the saliva volumes at specific time intervals (30 min, 60 min, 90 min, 120 min, and 150 min) were measured for each group of SD rats. Data are presented as the mean ± S.D., n = 6. $^{*}p < 0.05$ *versus* control group; $^{\#}p < 0.05$ *versus* model group.

expression in the submandibular glands, improved glandular function, and enhanced saliva secretion. Notably, the medium- and high-dose groups demonstrated effects comparable to those of the positive control, indicating encouraging therapeutic potential.

https://doi.org/10.2147/DDDT.S526278

STHJ Improved Xerostomia in a SjD Mouse Model (BALB/c Mice)

This study aimed to evaluate the therapeutic effects of STHJ in a SjD mouse model using BALB/c mice. Assessments included histological staining (HE and Masson's trichrome), Western blot of AQP5 expression, saliva output measurements, and organ weight evaluation across three independent batches. Mice were assigned to six groups: normal control, model, positive control (pilocarpine), and STHJ low-, medium-, and high-dose groups.

Treatment began on Day 28 post-immunisation and continued for 14 days. As shown in Figure 3A–C, the model group exhibited significant pathological changes in the submandibular glands, including acinar atrophy and inflammation. These changes were notably alleviated in the medium- and high-dose STHJ groups, while the low-dose group showed milder improvements. The positive control group demonstrated similar effects to the high-dose group. As shown in Supplementary Material Table S1, the analysis of inflammation scores (Focus scores) revealed a significant reduction in inflammation in the Pilocarpine and High Dose groups compared to the Model Control group.

Masson's staining (Figure 3D) showed pronounced fibrosis in the model group, whereas collagen deposition was substantially reduced in the medium- and high-dose STHJ groups, resulting in tissue morphology resembling that of the normal controls. Fibrosis remained more evident in the low-dose group.

Western blot analysis (Figure 3E) revealed significantly reduced AQP5 expression in the model group. All STHJ dose groups significantly increased AQP5 levels in a dose-dependent manner ($p < 0.05$), with the high-dose group achieving expression levels close to or exceeding those in the positive control.

Saliva secretion was also markedly decreased in the model group (Figure 3F). STHJ treatment, particularly at medium and high doses, significantly enhanced saliva production ($p < 0.05$). The high-dose group performed comparably to the positive control, while the low-dose group showed a modest but less pronounced effect.

Submandibular gland and heart weights (Figure 3G) were slightly reduced in the model group, but differences among the groups were not statistically significant, suggesting these parameters may not be sensitive markers under the current conditions.

Overall, the findings indicate that STHJ may help alleviate SjD-associated xerostomia in mice, likely through AQP5 upregulation, reduced glandular fibrosis, and improved saliva secretion, with more pronounced effects at higher doses.

STHJ Ameliorated Inflammation and Immune Infiltration in a SjD Mouse Model (BALB/c Mice)

To explore the anti-inflammatory effects of STHJ, immunofluorescence staining and quantitative image analysis were conducted on submandibular gland sections. As shown in Figure 4A and B, quantitative evaluation of integrated fluorescence density revealed a significant increase in the number of $B220^+$ B cells, $CD4^+$ T cells, and $CD8^+$ T cells in the model group compared to controls ($p < 0.05$), accompanied by a marked reduction in $CD4^+Foxp3^+$ regulatory T cells. These changes were substantially reversed in the medium- and high-dose STHJ groups, as confirmed by image-based quantification using ImageJ software.The low-dose group exhibited partial improvement, while the positive control group showed results similar to those of the high-dose group.

ELISA data (Figure 4C) confirmed elevated levels of TNF-α, TNF-β, IFN-γ, IL-6, anti-SSA/Ro, and anti-SSB/La in the model group, reflecting an enhanced inflammatory response. STHJ administration significantly reduced the levels of these cytokines, especially TNF-α and IL-6 ($p < 0.05$). The low-dose group produced moderate reductions, while the positive control achieved similar effects to the medium-dose group.

Together, these results support the notion that STHJ exerts anti-inflammatory and immunoregulatory effects in this SjD mouse model, particularly at medium and high doses.

STHJ Ameliorated Inflammation in a SjD Mouse Model (BALB/c Mice) via Inhibition of MAPK p38 and NF-κB Signalling

To further investigate the anti-inflammatory mechanism of STHJ, we examined the expression of key proteins in the MAPK p38 and NF-κB pathways via immunofluorescence and Western blot (Figure 5A and B). The model group showed significantly increased phosphorylation of IKKβ, p65, p38, and IKBα, indicating activation of both pathways.

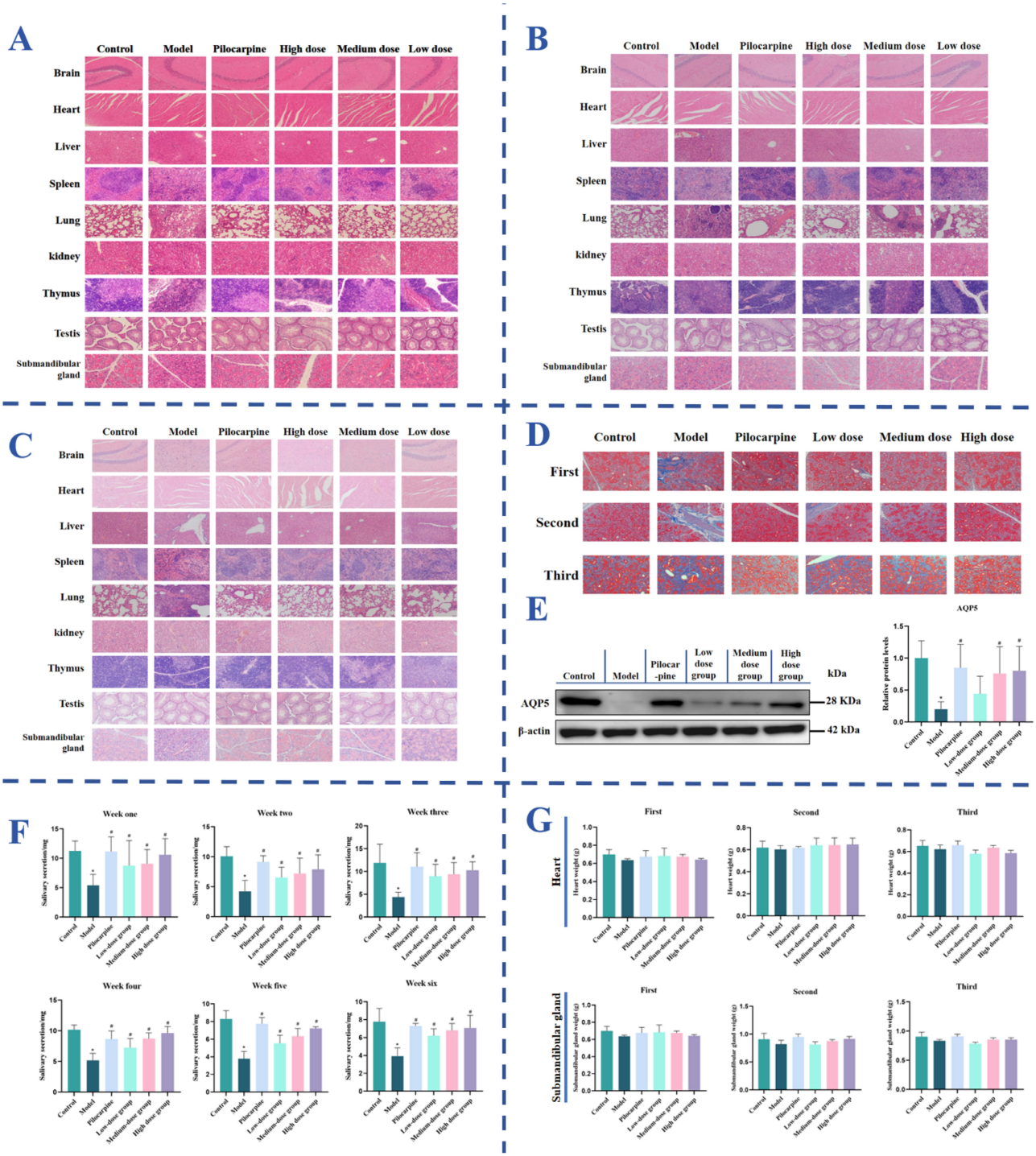

Figure 3 STHJ Improved Xerostomia in a SjD Mouse Model (BALB/c Mice). (**A**–**C**) Tissue sections from the heart, liver, spleen, lungs, kidneys, brain, testes, submandibular glands, and thymus of three batches of mice were prepared and subjected to histopathological examination following HE staining. (**D**) The degree of fibrosis in the submandibular glands was evaluated using Masson's trichrome staining. (**E**) The expression of AQP5 in the submandibular glands was determined by Western blot analysis. Data are presented as the mean ± S.D., n = 5. $^{*}p < 0.05$ versus control group; $^{\#}p < 0.05$ versus model group. (**F**) Saliva volume was measured in all three batches of mice. Data are presented as the mean ± S.D., n=10 (week one and week two), n=7 (week three and week four), n = 4 (week five and week six). $^{*}p < 0.05$ versus control group; $^{\#}p < 0.05$ versus model group. (**G**) The weights of the hearts and submandibular glands were assessed in the three batches of mice. Data are presented as the mean ± S.D., n = 3 (first and second), n = 4 (third).

https://doi.org/10.2147/DDDT.S526278

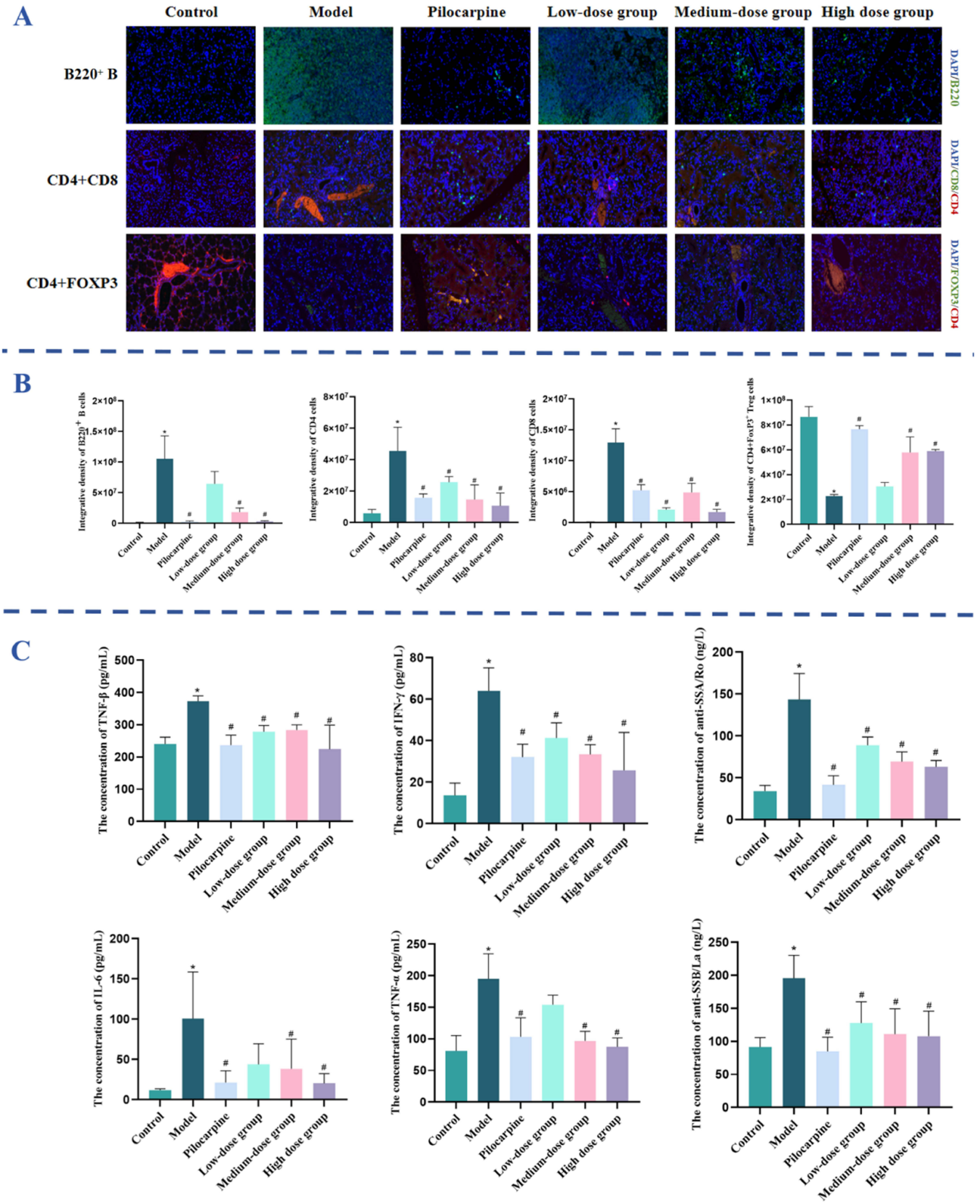

Figure 4 STHJ Ameliorated Inflammation and Immune Infiltration in a SjD Mouse Model (BALB/c Mice). (**A** and **B**) The expression levels of $B220^+$ B cells, $CD4^+$ T cells, and $CD8^+$ T cells in the submandibular glands of mice were assessed using immunofluorescence. Data are presented as the mean ± S.D., n = 5. *$p < 0.05$ *versus* control group; #$p < 0.05$ *versus* model group. (**C**) The levels of TNF-α, TNF-β, IFN-γ, IL-6, anti-SSA/Ro and anti-SSB/La were measured using ELISA. Data are presented as the mean ± S.D., n = 4. *$p < 0.05$ *versus* control group; #$p < 0.05$ *versus* model group.

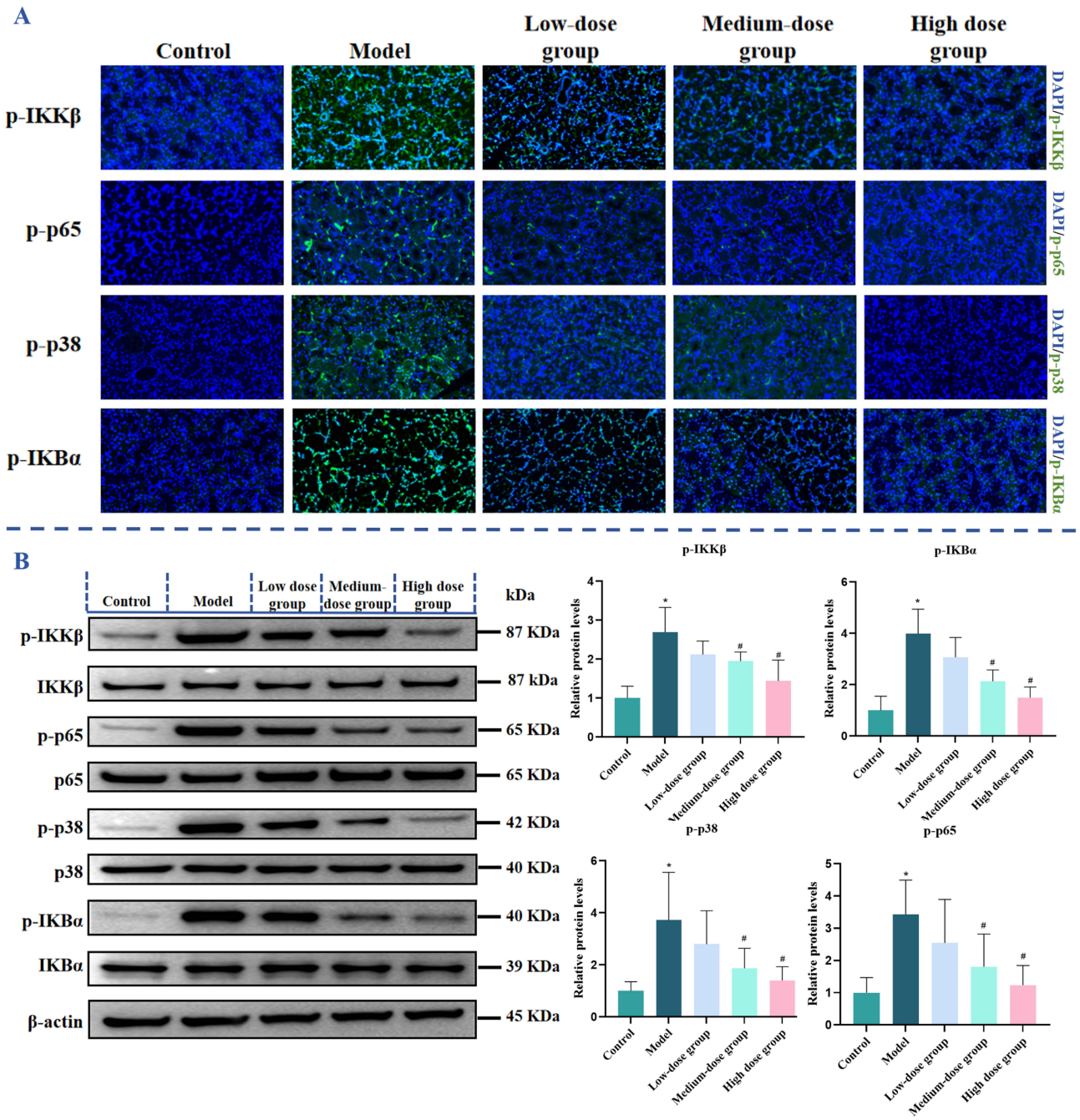

Figure 5 STHJ Ameliorated Inflammation in a SjD Mouse Model (BALB/c Mice) via Inhibition of MAPK p38 and NF-κB signalling Pathways. The expression levels of key proteins in the MAPK p38 and NF-κB signalling pathways, including p-IKKβ/IKKβ, p-p65/p65, p-p38/p38, and p-IKBα/IKBα, were assessed using immunofluorescence (**A**) and Western blot analysis (**B**). Data are presented as the mean ± S.D., n = 5. *$p < 0.05$ *versus* control group; #$p < 0.05$ *versus* model group.

Treatment with medium- and high-dose STHJ significantly suppressed phosphorylation of these proteins ($p < 0.05$), suggesting inhibition of pathway activation. The low-dose group exhibited some reduction, but the changes were not statistically significant.

In summary, these results suggest that STHJ may alleviate inflammation in SjD by downregulating phosphorylation of key signalling molecules in the NF-κB and MAPK p38 pathways.

https://doi.org/10.2147/DDDT.S526278

Table 13 Analysis of Acute Toxic Blood Cells in Each Group of SD Rats

Parameter	Control		Low Dose Group		Medium Dose Group		High-Dose Group	
	Average	RSD	Average	RSD	Average	RSD	Average	RSD
Hemameba number	3.60	0.39	3.96	0.33	3.54	0.25	2.60	0.49
Neutrophile number granulocyte number	0.75	0.76	1.04	0.49	1.02	0.29	0.62	0.50
Lymphocytenumber	2.33	0.31	2.01	0.34	1.84	0.28	1.57	0.46
Monocyte number	0.48	0.60	0.89	0.51	0.66	0.34	0.40	0.61
Eosinophils number	0.04	0.20	0.02	0.82	0.01	0.35	0.01	0.39
Basophilic granulocyte number	0.00	2.45	0.01	1.10	0.01	0.39	0.01	1.67
Neutrophile granulocytenumber	19.48	0.39	24.92	0.23	28.50	0.11	23.65	0.13
Percentage of Lymphocytes	66.50	0.15	57.37	0.14	54.05	0.06	61.03	0.07
Percentage of lymphocytes	12.85	0.21	17.12	0.16	16.72	0.05	14.63	0.12
Percentage of eosinophils	1.07	0.25	0.35	0.69	0.33	0.56	0.53	0.28
Percentage of basophils	0.08	1.59	0.23	1.11	0.37	0.37	0.12	1.57
Number of red cells	7.10	0.03	7.27	0.08	6.91	0.09	7.01	0.12
Hemoglobin	149.67	0.04	150.67	0.07	143.33	0.14	144.00	0.11
Accumulation of red blood cells	45.48	0.05	47.08	0.10	43.00	0.11	43.75	0.14
Mean corpuscular volume	64.13	0.04	64.75	0.03	62.15	0.04	62.42	0.06
Mean corpuscular hemoglobin content	21.10	0.05	20.75	0.03	20.67	0.09	20.60	0.06
Mean corpuscular-hemoglobin concentration	329.33	0.03	320.83	0.05	332.17	0.06	330.50	0.07
Coefficient of variation of red cell distribution width	15.30	0.06	14.40	0.03	14.33	0.06	14.32	0.07
Standard deviation of red blood cell distribution width	34.80	0.11	34.83	0.11	36.27	0.09	35.42	0.10
Platelet count	1104.67	0.08	973.83	0.12	1057.67	0.10	845.00	0.40
Mean platelet volume	6.40	0.05	6.43	0.12	6.20	0.08	6.67	0.06
Platelet distribution width	15.75	0.01	16.12	0.06	15.60	0.01	15.73	0.03
Thrombocytocrit	0.71	0.08	0.62	0.12	0.65	0.05	0.57	0.43

STHJ Exhibited no Toxicity in SD Rats

To assess the safety of STHJ, we conducted an acute toxicity study in SD rats. No abnormal clinical signs or behavioural changes were observed during the treatment period. All rats maintained normal feeding, activity, and responses to stimuli.

Haematological parameters (Table 13) and biochemical markers (ALT, AST, UREA, CREA; Figure 6A) remained within normal ranges across all treatment groups, with no significant differences compared to controls.

Necropsy revealed no macroscopic abnormalities. Histological examination (Figure 6B) confirmed the absence of tissue damage or pathological alterations in major organs, including the heart, liver, kidneys, lungs, brain, and submandibular glands.

These findings suggest that STHJ does not induce acute toxicity under the tested conditions and is well tolerated in SD rats.

Discussion

In this study, we conducted a systematic analysis of the quality control of STHJ, with particular emphasis on identifying its components using TLC. STHJ comprises twelve traditional Chinese medicines, including *Radix Adenophorae, Radix Pseudostellariae, Radix Rehmanniae, Radix Astragali, Herba Dendrobii, Radix Ophiopogonis, Fructus Lycii, Bombyx Batryticatus, Prunella Vulgaris, Triticum Aestivum, Fructus Jujubae and Radix Glycyrrhizae*. We performed TLC identification experiments on the main chemical constituents of these medicines, confirming the presence of these active ingredients in the tested samples. This finding demonstrates the consistency of the chemical composition of STHJ with its herbal reference materials, further ensuring the stability of the quality of this compound preparation. Additionally, we explored the impact of sucrose content on the pH value and relative density of STHJ. The results indicated that, within the studied range, sucrose had minimal effect on the quality characteristics of the preparation. In summary, this study

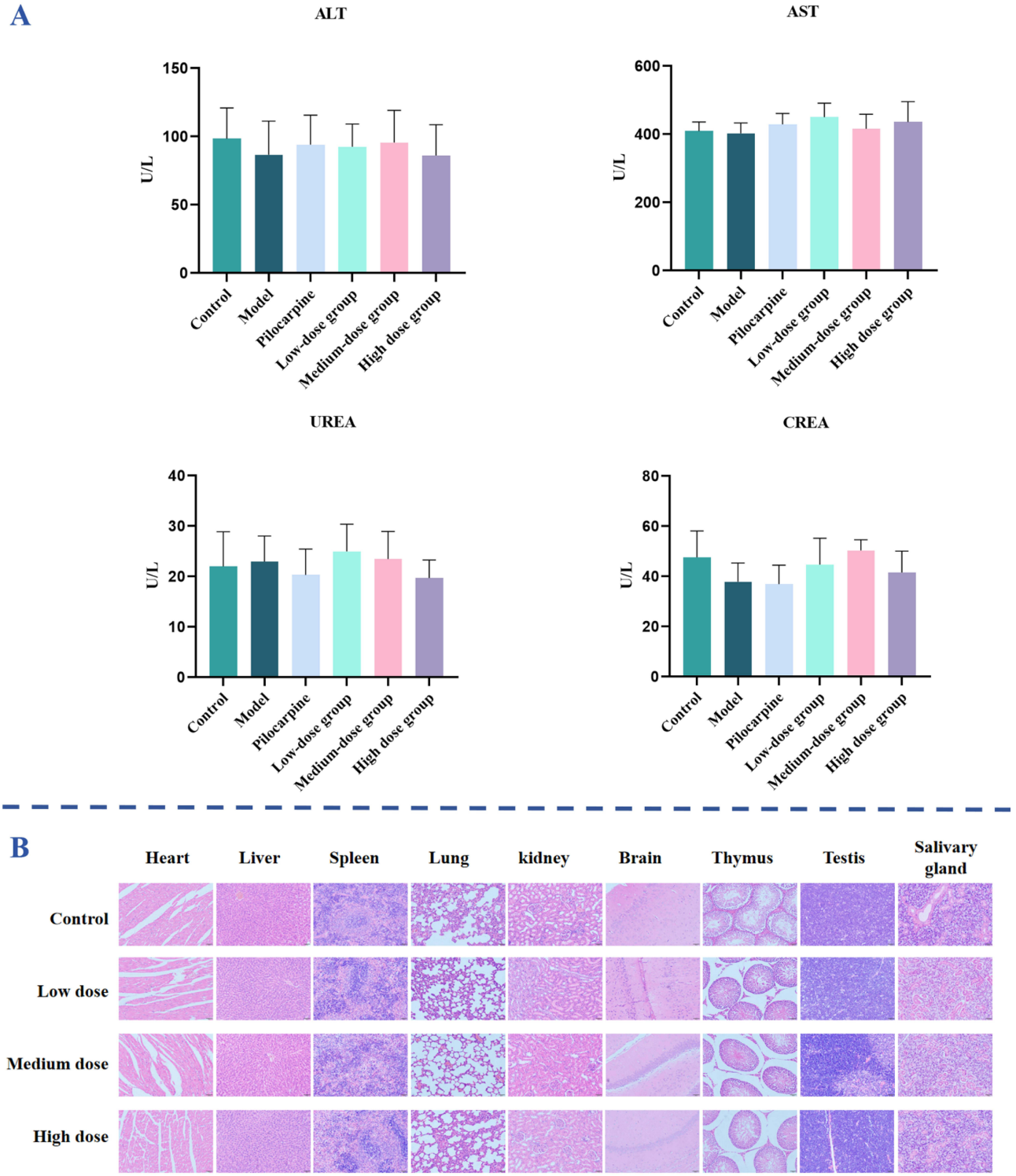

Figure 6 STHJ Exhibited No Toxicity in SD Rats. (**A**) The levels of ALT, AST, UREA, and CREA were measured in each group. Data are presented as the mean ± S.D., n = 6. (**B**) The heart, liver, spleen, lungs, kidneys, brain, testes, submandibular glands, and thymus were excised from the rats, sectioned, and subjected to HE staining for histopathological analysis.

https://doi.org/10.2147/DDDT.S526278

verified the composition of STHJ using TLC technology, ensuring consistency in drug quality. Further system suitability testing revealed that the analysis system used was appropriate for evaluating *Radix Astragali* and *Radix Rehmanniae*, providing a solid foundation for the quality control and standardisation of STHJ.

SjD is an autoimmune disease often associated with significant submandibular gland dysfunction.[16] Research indicates that the expression of AQP5 in the submandibular glands of SjD patients is significantly reduced, which correlates closely with the severity of xerostomia symptoms.[17] In our study, we first evaluated the efficacy of STHJ in an SD rat model of M receptor antagonist-induced xerostomia. Atropine, a well-known muscarinic receptor antagonist, reduces salivary secretion by blocking parasympathetic cholinergic signalling,[18] thus serving as a pharmacological mimic of hyposalivation in humans.[19,20] Pilocarpine was used as a positive control, as it activates M3 receptors to enhance salivation and is clinically used to treat xerostomia.[21,22]

Histopathological analyses and Western blotting confirmed that AQP5 expression was significantly reduced in model rats, validating the model. STHJ treatment, particularly at medium and high doses, restored AQP5 expression and improved salivary secretion in a dose-dependent manner. Moreover, no significant differences were observed in ALT, AST, UREA, and CREA levels between treated and control groups, suggesting minimal hepatic or renal toxicity. These results indicate that STHJ improves glandular function and has a favourable short-term safety profile.

To further investigate the efficacy of STHJ in autoimmune-related xerostomia, we used a BALB/c mouse model of SjD. This model is based on repeated immunisation with submandibular gland antigen and CFA, triggering lymphocytic infiltration and glandular damage consistent with human SjD.[14] Histological examination revealed significant inflammatory infiltration and acinar atrophy in the model group, which were alleviated by STHJ, particularly in the medium- and high-dose groups. Masson staining confirmed fibrosis in the submandibular glands of model mice, which was significantly reduced in the STHJ-treated groups.

Western blot analysis showed that AQP5 expression was significantly restored by STHJ in a dose-dependent manner. Repeated saliva secretion testing across three batches of mice consistently showed improved secretion in treated groups, with high-dose STHJ achieving levels close to the normal control. Interestingly, no significant changes in submandibular gland or heart weight were observed, suggesting that gland weight may not be a sensitive marker for therapeutic efficacy in this model.

We further explored the immune mechanisms underlying the therapeutic effects. Immunofluorescence analysis demonstrated increased infiltration of $B220^+$ B cells, $CD4^+$ and $CD8^+$ T cells, and a decrease in $CD4^+FOXP3^+$ Treg cells in model mice. These changes were reversed by STHJ treatment, suggesting immunomodulatory activity. ELISA results showed significantly elevated TNF-α, TNF-β, IFN-γ, IL-6, anti-SSA/Ro, and anti-SSB/La in model animals, consistent with SjD pathology.[5,23,24] STHJ significantly reduced these cytokines and autoantibodies, particularly in medium- and high-dose groups, indicating its anti-inflammatory and immunosuppressive potential.

Mechanistically, we confirmed that the NF-κB and MAPK p38 pathways were activated in SjD model mice, as shown by increased phosphorylation of p65, IKKβ, IκBα, and p38 (as illustrated in Figure 7). STHJ treatment inhibited these

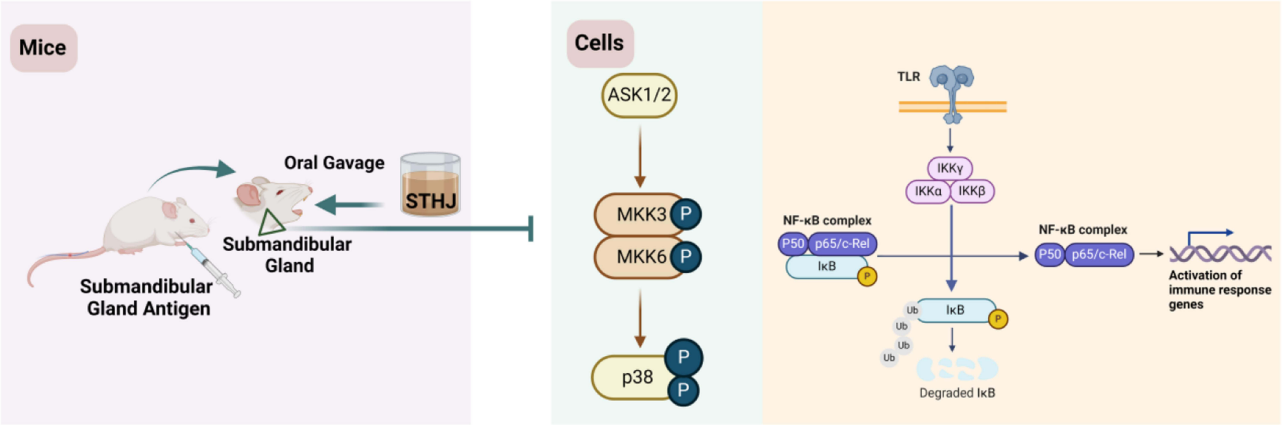

Figure 7 STHJ alleviated inflammation in a SjD mouse model (BALB/c mice) by suppressing the MAPK p38 and NF-κB signalling pathways. Created in BioRender. Liu, F. (2025) https://BioRender.com/lv278p7.

activations in a dose-dependent manner, indicating that its therapeutic effects may be mediated by suppressing key inflammatory signalling cascades, consistent with previous studies on the central role of these pathways in SjD.

We also conducted acute toxicity testing in SD rats. No abnormal behavioural signs, organ damage, or histopathological changes were observed. Blood biochemistry and haematology parameters remained within normal ranges across all dose groups, further supporting the short-term safety of STHJ.

This study has several limitations. First, the observation period was relatively short, and long-term efficacy and safety remain unconfirmed. Second, we did not assess correlations between biomarker levels and clinical endpoints such as glandular weight or histological score. Third, while promising, these findings are preclinical, and caution is warranted in extrapolating to human use.

Conclusion

In conclusion, we established the quality control standards for STHJ and conducted a comprehensive evaluation of its pharmacodynamic properties, safety profile, and potential mechanisms of action. The therapeutic effects of STHJ were investigated using an M receptor antagonist-induced xerostomia model in SD rats and a SjD model in BALB/c mice. In the SD rat model, STHJ markedly increased AQP5 expression in the submandibular glands, improved glandular structure, and enhanced saliva secretion. In the SjD mouse model, STHJ demonstrated notable anti-inflammatory and immunomodulatory effects. It reduced autoantibody levels against anti-SSA/Ro and anti-SSB/La, alleviated lymphocyte infiltration, inhibited the expression of pro-inflammatory cytokines such as TNF-α and IL-6, and modulated Treg cell proportions, reflecting a multifaceted therapeutic profile. These effects were particularly evident in the medium- and high-dose groups. Mechanistic studies further indicated that the anti-inflammatory actions of STHJ may involve inhibition of the MAPK p38 and NF-κB signalling pathways.

Collectively, these findings suggest that STHJ possesses favourable pharmacological properties and a favourable safety profile in preclinical settings, supporting its potential as a candidate for further development in the management of xerostomia associated with SjD and related conditions.

Abbreviations

CFA, complete Freund's adjuvant; HE, haematoxylin-eosin; NK, natural killer; SD, Sprague-Dawley; SjD, Sjögren disease; STHJ, Shatai Heji; TCM, traditional Chinese medicine; TLC, thin-layer chromatography; TNF-α, tumour necrosis factor-α.

Acknowledgments

We would like to thank all the authors who participated in the present study, as well as the reviewers of this paper for their valuable comments and guidance.

The graphical abstract was Created in BioRender. Liu, F. (2025) https://BioRender.com/lv278p7.

Author Contributions

All authors made a significant contribution to the work reported, whether in the conception, study design, execution, acquisition of data, analysis, or interpretation; took part in drafting, revising, or critically reviewing the article; gave final approval of the version to be published; have agreed on the journal to which the article has been submitted; and agree to be accountable for all aspects of the work.

Funding

This study was supported by Science and Technology Commission of Shanghai Municipality (Grant No. 22S21901700). We thank Elsevier LTD for its linguistic assistance.

Disclosure

Mr Jiyuan Chen reports a patent CN119318687A pending to China National Intellectual Property Administration. The authors report no other conflicts of interest in this work.

References

1. Lee AYS. Serum α-amylase correlates with xerostomia in patients with primary Sjögren's disease. *Int J Rheum Dis*. 2024;27(8):e15313. doi:10.1111/1756-185X.15313
2. Jeon SG, Lee J, Lee SJ, et al. Salivary gland organoid transplantation as a therapeutic option for radiation-induced xerostomia. *Stem Cell Res Ther*. 2024;15(1):265. doi:10.1186/s13287-024-03833-x
3. Alkahtani A, Grootveld M, Bhogadia M, Baysan A. Exploring salivary metabolic alterations in type 2 diabetes: implications for dental caries and potential influences of HbA1c and vitamin D levels. *Metabolites*. 2024;14(7):372. doi:10.3390/metabo14070372
4. Houen G. Auto-immuno-deficiency syndromes. *Autoimmun Rev*. 2024;23(9):103610. doi:10.1016/j.autrev.2024.103610
5. Afzali AM, Moog P, Kalluri SR, et al. CNS demyelinating events in primary Sjögren's syndrome: a single-center case series on the clinical phenotype. *Front Neurol*. 2023;14:1128315. doi:10.3389/fneur.2023.1128315
6. De Vita S, Isola M, Baldini C, et al. Predicting lymphoma in Sjögren's syndrome and the pathogenetic role of parotid microenvironment through precise parotid swelling recording. *Rheumatology*. 2023;62(4):1586–1593. doi:10.1093/rheumatology/keac470
7. Wiseman LR, Faulds D. Oral pilocarpine: a review of its pharmacological properties and clinical potential in xerostomia. *Drugs*. 1995;49(1):143–155. doi:10.2165/00003495-199549010-00010
8. Li H, Liu Z, Liu Q, et al. Extraction of polysaccharides from root of Pseudostellaria heterophylla (Miq.) Pax and the effects of ultrasound treatment on its properties and antioxidant and immune activities. *Molecules*. 2023;29(1):142. doi:10.3390/molecules29010142
9. Lin R, Hao D, Dong Y, Wang Y. Catalpol ameliorates Sjögren's syndrome by modulating interplay of T and B cells. *Biomed Pharmacother*. 2020;123:109806. doi:10.1016/j.biopha.2019.109806
10. Wu M, Yu S, Chen Y, et al. Acteoside promotes B cell-derived IL-10 production and ameliorates autoimmunity. *J Leukoc Biol*. 2022;112(4):875–885. doi:10.1002/JLB.3MA0422-510R
11. Wang F, Lui J, Ye Y, Zhang X, Wan L, Li Z. Astragalus polysaccharides improved the cardiac function in Sjögren's syndrome model rats based on keap1-Nrf2/ARE signaling pathway: a mechanism exploration. *Zhongguo Zhong Xi Yi Jie He Za Zhi*. 2014;34(5):566–574. doi:10.7661/CJIM.2014.05.0566
12. Ding YM, Hu BP, Guo YQ. Treatment of Sjögren's syndrome with self made SS sirup. *Shanghai Kou Qiang Yi Xue*. 1995;4(3):143–144.
13. Fan K. Study on the immunoregulatory effects and mechanisms of Fufang Shatai Heji dissertation. Shanghai: Shanghai Jiao Tong University; 2019. doi:10.27307/d.cnki.gsjtu.2019.003579.
14. Lee BH, Gauna AE, Pauley KM, Park YJ, Cha S. Animal models in autoimmune diseases: lessons learned from mouse models for Sjögren's syndrome. *Clin Rev Allergy Immunol*. 2012;42(1):35–44. doi:10.1007/s12016-011-8288-5
15. Chen Q, Li M, Yang J. Sjögren's syndrome traditional Chinese medicine formula cluster analysis. *China J Tradit Chin Med Pharm*. 2015;30(7):2601–2603.
16. Florezi GP, Barone FP, Izidoro MA S-J-JM, Coutinho-Camillo CM, Lourenço SV. Targeted saliva metabolomics in Sjögren's syndrome. *Clinics*. 2024;79:100459. doi:10.1016/j.clinsp.2024.100459
17. Chivasso C, C D, Parisis D, Soyfoo MS, Delporte C. Involvement of aquaporin 5 in Sjögren's syndrome. *Autoimmun Rev*. 2023;22(3):103268. doi:10.1016/j.autrev.2023.103268
18. Prathumsap N, Ongnok B, Khuanjing T, et al. Muscarinic and nicotinic receptors stimulation by vagus nerve stimulation ameliorates trastuzumab-induced cardiotoxicity via reducing programmed cell death in rats. *Toxicol Appl Pharmacol*. 2024;491:117074. doi:10.1016/j.taap.2024.117074
19. Nihei Y, Haniuda K, Higashiyama M, et al. Identification of IgA autoantibodies targeting mesangial cells redefines the pathogenesis of IgA nephropathy. *Sci Adv*. 2023;9(12):eadd6734. doi:10.1126/sciadv.add6734
20. Schwartz MD, Raulli R, Laney JW, et al. Systemic bioavailability of sublingual atropine ophthalmic solution: a phase I study in healthy volunteers with implications for use as a contingency medical countermeasure. *J Med Toxicol*. 2022;18(3):187–197. doi:10.1007/s13181-021-00873-0
21. Komuro A, Yokoi N, Sotozono C, Kinoshita S. Effectiveness of single-dose oral pilocarpine administration in patients with Sjögren's syndrome. *Diagnostics*. 2023;14(1):91. doi:10.3390/diagnostics14010091
22. Wang K, Xie Y, Chen X, et al. The activation of muscarinic acetylcholine receptors protects against neuroinflammation in a mouse model through attenuating microglial inflammation. *Int J Mol Sci*. 2024;25:10432. doi:10.3390/ijms251910432
23. Luciani GR, Barilli A, Visigalli R, V D, Rotoli BM. Cytokines from SARS-CoV-2 Spike-activated macrophages hinder proliferation and cause cell dysfunction in endothelial cells. *Biomolecules*. 2024;14(8):927. doi:10.3390/biom14080927
24. Deroo L, Achten H, Boeck KD, et al. The value of separate detection of anti-Ro52, anti-Ro60 and anti-SSB/La reactivities in relation to diagnosis and phenotypes in primary Sjögren's syndrome. *Clin Exp Rheumatol*. 2022;40(12):2310–2317. doi:10.55563/clinexprheumatol/l70874

Drug Design, Development and Therapy

Dovepress
Taylor & Francis Group

Publish your work in this journal

Drug Design, Development and Therapy is an international, peer-reviewed open-access journal that spans the spectrum of drug design and development through to clinical applications. Clinical outcomes, patient safety, and programs for the development and effective, safe, and sustained use of medicines are a feature of the journal, which has also been accepted for indexing on PubMed Central. The manuscript management system is completely online and includes a very quick and fair peer-review system, which is all easy to use. Visit http://www.dovepress.com/testimonials.php to read real quotes from published authors.

Submit your manuscript here: https://www.dovepress.com/drug-design-development-and-therapy-journal